Atmos. Chem. Phys. Discuss., doi:10.5194/acp-2016-824, 2016
Manuscript under review for journal Atmos. Chem. Phys.
Published: 8 November 2016

Atmospheric Chemistry and Physics Discussions

Transport of regional pollutants through a remote trans-Himalayan valley in Nepal

Shradda Dhungel[1], Bhogendra Kathayat[2], Khadak Mahata[3], Arnico Panday[1,4]

[1] Department of Environmental Sciences, University of Virginia, Charlottesville, VA 22904, USA
[2] Nepal Wireless, Shanti Marg, Pokhara, 33700, Nepal
[3] Institute for Advanced Sustainability Studies, Potsdam, 14467, Germany
[4] International Center for Integrated Mountain Development, Khulmaltar, Kathmandu, 44700, Nepal

Correspondence to: Shradda Dhungel (shradda@virginia.edu)

Abstract. Anthropogenic emissions from the combustion of fossil fuels and biomass in Asia have increased in recent years. High concentrations of reactive trace gases and absorbing and light-scattering particles from these sources over the Indo-Gangetic Plain (IGP) of southern Asia form persistent haze layers, also known as atmospheric brown clouds, from December through early June. Models and satellite imagery suggest that strong wind systems within deep trans-Himalayan valleys are major pathways by which pollutants over the IGP are transported to the high Tibetan Plateau (TP). To evaluate this pathway, we measured black carbon (BC), ozone (O_3), and associated meteorological conditions within the Kali-Gandaki Valley, Nepal, from January 2013 to August 2015. BC and O_3 varied over both diurnal and seasonal cycles. Relative to nighttime, mean BC and O_3 concentrations within the valley were higher during daytime when the up-valley flow (average velocity of 17 ms^{-1}) dominated. Minimal BC and O_3 concentrations occurred during the monsoon season (July to September). Concentrations of both species subsequently increased post monsoon and peaked during March to May. We recorded average concentration for O_3 during April, July, and November were 41.7 ppbv, 24.5 ppbv, and 29.4 ppbv, respectively, while the corresponding BC concentrations were 1.17 µg m^{-3}, 0.24 µg m^{-3}, and 1.01 µg m^{-3}, respectively. Frequent episodes of concentrations two to three fold higher than average persisted from several days to a week during non-monsoon months. Our observations of increases in BC concentration in the valley - especially during pre-monsoon season (April) - support the hypothesis that trans-Himalayan valleys are important conduits for transport of pollutants from the IGP to TP. In addition, the increase in BC concentration in the KGV during high fire activity in Northern India and southern Nepal corroborates the role of trans-Himalayan valleys as vital pollutant transport pathways.

Keywords: black carbon, ozone, trans-Himalayan valleys, pollutant pathways, long-range transport, regional transport episodes, short-lived climate forcers.

Atmos. Chem. Phys. Discuss., doi:10.5194/acp-2016-824, 2016
Manuscript under review for journal Atmos. Chem. Phys.
Published: 8 November 2016

Atmospheric Chemistry and Physics Discussions

1. Introduction

Persistent atmospheric haze, often referred to as Atmospheric Brown Clouds (ABC) (Ramanathan and Crutzen, 2003), affects broad geographic regions including the Indo-Gangetic plain (IGP) in southern Asia (Ramanathan and Carmichael, 2008), eastern China (Ma et al., 2010), southeast Asia (Engling and Gelencser, 2010), sub-Saharan Africa (Piketh et al., 1999), Mexico (Vasilyev et al., 1995), and Brazil (Kaufman et al., 1998). In southern Asia, the haze covers extensive areas particularly during the period of mid-November to mid-June that precedes the summer monsoon season. Major combustion sources (primarily anthropogenic) including wildfires and the burning of agricultural waste, garbage, biofuel, and fossil fuels emit volatile and particulate-phase compounds to the atmosphere that contain oxidized and reduced forms of sulfur, nitrogen, and organic carbon (OC) together with elemental (black) carbon (BC) and minerals. These emissions are intermixed and chemically interact with mechanically produced aerosols (e.g. sea salt and mineral dust). Important secondary pollutants such as ozone (O_3) from photochemical reactions involving nitrogen oxides are also produced. Together, this mixture of atmospheric species constitutes ABC or the brown haze in South Asia (Ramanathan et al., 2005; Gustafsson et al., 2009). These optically thick layers include high concentrations of light absorbing and light scattering particles (Menon et al., 2002) that modulate radiative transfer. Light absorbing aerosols (primarily BC and mineral dust) contribute to warming of the atmosphere while light scattering aerosols (primarily S-, N-, and OC dominated particles) drive cooling at the surface. The combined effects of light absorbing and light scattering aerosols from anthropogenic sources reduce UV and visible wavelength radiation at the surface (i.e., surface forcing), increase the warming of the troposphere (i.e., atmospheric forcing) and change the net top of the atmosphere solar flux (i.e., top-of-the-atmosphere forcing) (Andreae and Crutzen, 1997; Kaufman et al., 2002, Ramanathan et al., 2005). Absorbing anthropogenic pollutants like BC significantly influence global warming, in terms of direct radiative forcing (Jacobson, 2001); regional influences from such pollutants close to sources are greater than those on the global scale (Ramanathan et al., 2007b). Ozone precursors including nitrogen oxides and volatile organic carbon (VOC) are emitted to the atmosphere together with BC from combustion sources. VOCs are also emitted from biogenic sources including microbial decomposition and vegetation. In addition, the downwelling of stratospheric ozone across the tropopause contributes to background levels of tropospheric O_3. Finally, O_3 is produced photochemically during the daytime whereas BC is a relatively inert primary emission product.

Air pollution from the source regions across the IGP, which extends along the southern side of the Himalaya from eastern Pakistan across northern India and southern Nepal to Bangladesh, often reach heights of more than 3 km above sea level via convection and advection (Ramanathan et al., 2007a). The radiative properties of associated aerosols influence the Asian summer monsoon (ASM) (Lau et al., 2006). The elevated concentration of aerosols in the anti-cyclone alters the strength of circulation pattern and reduces total monsoon precipitation over southern India (Ramanathan et al, 2005; Fadnavis et al., 2013) while intensifying the monsoon over the foothills of the Himalaya (Lau et al., 2006). BC and O_3 concentrations are rising in response to increasing emissions over southern Asia (Ramanathan

Atmos. Chem. Phys. Discuss., doi:10.5194/acp-2016-824, 2016
Manuscript under review for journal Atmos. Chem. Phys.
Published: 8 November 2016

Atmospheric Chemistry and Physics Discussions

and Carmichael, 2008). In addition to warming the atmosphere, both pollutants also have detrimental impacts on human health. The effects of BC on cardiopulmonary and respiratory problems are greater than those of PM 2.5 or 10 particles (Janssen et al., 2011). O_3 also compromises pulmonary function (Krupnick et. al, 1990) and is a leading pollutant causing biodiversity loss (Royal Society, 2008) and declining crop yields by directly damaging leaves (Auffhammer et al., 2006).

Most haze over the IGP is in the lower 3 km of the atmosphere, and the Himalaya range forms a 2500 km long complex topographic barrier along the northern edge of the IGP extending more than 8 km high. However, satellite imagery (Ramanathan et al., 2007a), back trajectories (Lu et al., 2011), model calculations (Kopacz et al., 2011), and ice core analyses (Lee et al., 2008, Kang et al., 2010) strongly suggest that pollutants are efficiently transported from the IGP to the Tibetan Plateau (TP), especially during spring prior to the monsoon. Aerosols from the IGP significantly impact the Himalaya and TP. Absorbing aerosols warm the atmosphere at high altitudes and, when deposited onto snow and ice surfaces, decrease albedo thereby substantially increasing the rate of glacial and snow melting (Kang et al., 2010). Model simulations (Qian et al., 2011) show that the absorbing aerosols change the surface radiative flux in the higher Himalaya and the TP by 5 to 25 W m^{-2} during the pre-monsoon months of April and May. Atmospheric and surface absorption of solar radiation drives the physical climate system and the associated biogeochemical cycles that sustain life on the Earth. The TP plays a vital role in regulating the regional climate due to its effect on the ASM and the hydrologic cycle. High atmospheric mixing ratios of O_3 during growing seasons can decrease yields of wheat, rice and legumes in regions with increased O_3 pollution (Wang and Mauzerall, 2004). The interrelated perturbations of the ABC on radiative transfer, air quality, the hydrologic cycle, and crop yields have important long-term implications for human health, food security, and economic activity over southern Asia.

Lüthi et al. (2015) found that synoptic circulation patterns, in combination with local weather phenomena, are associated with the transport of polluted air masses from the IGP to the TP. However, to date, there has been little research on how air pollutants from the IGP and the Himalayan foothills cross the topographic barrier to reach the TP. Even during the absence of strong synoptic patterns, satellite imagery show IGP haze penetrating deep into mountain valleys on the south side of the Himalayan range (Brun et al., 2011). Well-known flow patterns carry polluted air masses up valleys to higher elevations by providing a path of least resistance between tall mountains. In the European Alps, prevailing wind systems in the mountain river valleys funnel polluted air from peripheral source regions to high elevations in a phenomenon known as “Alpine Pumping” (Weissmann et al., 2005). Relative to air over plains, the air within the valleys heats and cools more quickly (Steinacker, 1984). The resultant differences in temperature create gradients in pressure and air density, which in turn drive the wind that transports air from the plains to higher-elevations during the daytime (Reiter and Tang 1984, Whiteman and Bian, 1998; Egger et al., 2000).

Several major trans-Himalayan valleys including the Arun Valley in eastern Nepal and the Kali Gandaki Valley (KGV) in western Nepal provide topographical connection for air masses from the

Atmos. Chem. Phys. Discuss., doi:10.5194/acp-2016-824, 2016
Manuscript under review for journal Atmos. Chem. Phys.
Published: 8 November 2016

Atmospheric Chemistry and Physics Discussions

south to the TP (Fig.1). In addition to synoptic transport over the Himalaya, MODIS (MODerate-resolution Imaging Spectroradiometer) and CALIPSO (Cloud-Aerosol Lidar and Infrared Pathfinder Satellite Observation) imagery reveal northward slanted transport of polluted air mass towards higher elevations in the trans-Himalayan Arun Valley (Brun et al, 2011). The KGV exhibits distinct diurnal wind pattern, with strong daytime up-valley flow and weak nighttime down-valley flow. Based on the average daytime wind speed, the valley is divided into three regions: the entrance, core, and exit (average wind speeds range from 5 to 10 m s^{-1}, 8 to 18 m s^{-1}, and less than 5 m s^{-1}, respectively) (Egger et al 2000). The strongest winds within the core region are most prevalent in the lower 1000 to 1500 m of the boundary layer in the valley (Egger et al, 2000; Zängl et al., 2000, Egger et al., 2002).

In 2011we established an atmospheric measurement station in Jomsom (28.87° N, 83.73° E, 2900 m asl) within the core region of the KGV along with automated weather stations up and down the valley from Jomsom. With the exception of aerosol optical depth measured as part of AERONET (AErosol RObotic NETwork) (Xu et al., 2015), no data from Jomsom have been reported previously. Here we report diurnal and seasonal trends in two climatically important pollutants – BC and O_3. Results are interpreted to evaluate the role of trans-Himalayan valleys as pathways for the transport of polluted air from the IGP to the TP.

2. Measurement Sites and Methods

2.1 Measurement Sites and Instrumentation

The KGV is located in the Dhaulagiri zone of western Nepal. Figure 1(a), shows the TP in the upper right, with the Himalayan arc, the Himalayan foothills of India, Nepal and Bhutan, and the haze covered IGP to the south. The intrusion of haze from the IGP into Himalayan valleys is clearly visible. KGV floor changes elevation from approx. 1100 m to 4000 m asl over a horizontal distance of 90 km (Fig. 1(b)). Passing between the two eight thousand meter peaks of Dhaulagiri and Annapurna, it forms one of the deepest valleys in the world. The valley is a narrow gorge at the lower end and opens up into a wider, arid basin half way up (Fig. 1(b)). The maximum width of the basin is approximately one kilometer. The orientation of KGV varies from the entrance to the exit. The valley is oriented southeasterly (~135°) to northwesterly (~315°) at Lete. The valley's orientation changes to southwesterly (~225°) to northeasterly (~45°) at Marpha. At Jomsom, the valley bends towards the east (~210°) and past Eklobhatti the valley turns north (~20°) (Fig. 1). Approximately 13,000 inhabitants in several small settlements sparsely populate the valley. Emission sources within the valley include biofuel combustion for cooking and fossil-fuel combustion by a few scattered off-road vehicles. A total of 5245 vehicles have been registered in Dhaulagiri Zone since 2008, but most are based in the southern towns of Kusma, Baglung, and Beni, below 1 km altitude, at the lowest left corner of the map in Figure 1(b) (DOTM, 2016).

Atmos. Chem. Phys. Discuss., doi:10.5194/acp-2016-824, 2016
Manuscript under review for journal Atmos. Chem. Phys.
Published: 8 November 2016

Atmospheric Chemistry and Physics Discussions

The atmospheric observatory at Jomsom (JSM_STA) is equipped with instruments to measure BC, O_3, carbon monoxide, aerosol optical depth, and meteorology (Table 1). The observatory is located on the southeast corner of a plateau jutting out from an east-facing slope about 100 m above the valley floor and with no major obstructions either up or down the valley.

BC was measured with a Thermo Multiangle Absorption photometer (MAAP), model 5012 that analyzes the modification of radiation fields in the forward and back hemisphere of a glass-fiber filter caused by deposited particles using a multi-angle photometer. MAAP was operated at a flow rate of 20 L min^{-1} and measures BC at 1-minute frequency. Hyvarinen (2013) illustrates the artifact in MAAP measurements in environments with high aerosol loading with an underestimation of concentration above 9 µg m^{-3}. Since the median monthly concentration were less than 1µg m^{-3} and 90th percentile below 2 µg m^{-3} for all seasons which is below the threshold of 9 µg m^{-3}, MAAP corrections were not applied. O_3 was measured with a 2B Tech model 205 via the attenuation of ultraviolet light at 254 nm passing through a 15 cm long absorption cell fitted with quartz windows. The instrument operates at a flow rate of 1.8 L min^{-1}.

The observations used in this study cover January 2013 to August 2015, but periodic power disruptions caused occasional data gaps. Measurements of carbon monoxide were suspended in late 2012 due to limited power supply. Unless otherwise noted, data reported herein correspond to periods when BC, O_3 and meteorological data were available simultaneously. Data are binned by season as follows: monsoon (July-September), post-monsoon (October-February) and pre-monsoon (March-June). Times correspond to Nepal's local time (LT) (UTC + 5.75 h). An automated weather station was installed on a ridge (3700 m) above the Jomsom observatory (JSM_1) and was operational from July 2012 to July 2015.

From March to May 2015, four additional automated weather stations were operated along a transect about 10 meters above and in the center of the valley floor where wind speeds are typically highest: near the entrance of the valley at Lete (LET), within the core at Marpha (MPH) and Jomsom (JSM_2), and near exit at Eklobhatti (EKL) (Fig. 1b). Power outages and instrument malfunction limited the durations of record at all sites. However, between 8th and 14th May, all stations operated simultaneously and the resulting data provide valuable information with which to evaluate diurnal variability of wind fields within the valley.

O_3, BC and meteorological data were averaged over 10 minute intervals. In order to characterize relative diurnal variability, O_3 and BC concentrations measured during a given month were normalized to a common scale ranging from 0 to 1 by subtracting the minimum for the month from each individual value and then dividing by the range for the month. The data were then binned into twenty-four, 1-hour increments and plotted.

Atmos. Chem. Phys. Discuss., doi:10.5194/acp-2016-824, 2016
Manuscript under review for journal Atmos. Chem. Phys.
Published: 8 November 2016

Atmospheric Chemistry and Physics Discussions

3. Results and Discussion

3.1 Seasonal variability in BC and O_3

All data generated during the measurement period were binned by month to evaluate the seasonal patterns of BC and O_3 (Fig. 2). Median concentrations of both species were systematically lower during monsoon months relative to the rest of the year. BC concentrations during the monsoon period relative to non-monsoon period were lower. We infer that the lower concentrations during the monsoon reflect the influences of reduced biomass burning and associated emissions coupled with more efficient removal via wet deposition during the monsoon. The highest median values and ranges for both species occurred during the pre-monsoon period. Representative months from each season, April 2013 (pre-monsoon), July 2015 (monsoon) and November 2014 (post-monsoon), were selected based on data availability and quality to evaluate aspects of temporal variability in more detail. O_3 varies seasonally in the KGV, with highest mixing ratios during the pre-monsoon season and lowest during the monsoon (Fig. 2 and 3). BC and O_3 in monsoon is relatively smaller to those of non-monsoon months due in part to the southwesterly air flow that brings cleaner marine air mass from the oceans and suppressed O_3 production under cloudy conditions during the monsoon season (Lawrence and Lelieveld, 2010).

Seasonal variability in BC concentration is evident across the IGP from urban to remote locations and up in the Himalayan valleys like at the KGV indicating a broad regional pattern. The seasonal peaks observed at KGV, a remote Himlayan valley, are consistent with patterns to stations across the IGP. For example high concentrations of BC have been reported in near-surface air across the IGP as well as in layers of the atmosphere at ~900 m asl and ~1200 m asl during the post-monsoon over Northern India (Tripathi et al, 2005; 2007). Sreekanth et al (2007) reported BC concentrations in Vishkhapatnam, in eastern India, at 8.01 µg m^{-3} in pre-monsoon and 1.67 µg m^{-3} during monsoon while Ramchandran et al (2007) observed BC concentrations in Ahmedabad, western India, of 0.8 µg m^{-3} during the monoon in July and increased to 5 µg m^{-3} during the post monsoon in January (Ramchandran et al, 2007). The Nepal Climate Observatory-Pyramid (NCO-P) station at the 5079 m asl in the Himalaya has also shown high seasonal trends for BC (0.444 (±0.443) µ gm^{-3} during pre-monsoon and 0.064 (±0.101) µ gm^{-3} during monsoon season and ozone concentrations 61 (±9) ppbv during pre-monsoon season and 39 (±10) ppbv during monsoon (Cristofanelli et al., 2010, Marinoni et al., 2013). These differences in sources, atmospheric chemistry and processing contribute to differential seasonal (and diurnal) patterns in BC and O_3 in the KGV. BC in the Himalaya region is closely linked with regional emissions from forest fires, agricultural burning, exhaust from diesel vehicles, gas-powered generator sets for power, power plants, and brick kilns over the IGP (Lawrence and Lelieveld, 2010).

3.2 Diurnal variability in BC and O_3

Normalized diurnal cycles of O_3 and BC reveal several distinct patterns (Fig. 3). Based on median values during all three periods, O_3 peaked during daytime and dropped to minimal levels before sunrise.

Atmos. Chem. Phys. Discuss., doi:10.5194/acp-2016-824, 2016
Manuscript under review for journal Atmos. Chem. Phys.
Published: 8 November 2016

Atmospheric Chemistry and Physics Discussions

However, in the pre-monsoon period, O_3 peaked in the late afternoon whereas in the post-monsoon, it peaked in the early afternoon. In addition, the normalized diurnal excursions were greater during the pre- and post-monsoon periods relative to the monsoon period. Finally, the 10th through 90th percentiles of the concentration range accounted for most of the normalized scale from 0 to 1 (Fig. 3).

In contrast, based on median values during all three periods, BC concentrations increased rapidly following sunrise, decreased during late morning, and then rose through the afternoon and early evening hours (Fig. 3). Relative diurnal variability was somewhat greater during the post- relative to the pre-monsoon periods and lower during the monsoon period. Notably, the 10th through 90th percentiles of the concentration range for most time intervals during the pre- and post monsoon periods fell within the lower half of the normalized range and those for the monsoon period fell within the lowest 10% of the normalized range. These skewed distributions reflect infrequent periods of relatively high BC concentrations during all three seasons.

Several factors contributed to differences in the diurnal variability of O_3 and BC. O_3 is produced photochemically during daytime and is lost via deposition to surfaces and chemical reactions. Consequently, O_3 typically peaked in the afternoon and decreased over night (Figure 3). The reduced radiation associated with increased cloud cover during the monsoon likely contributed to the relatively lower diurnal variability during that period relative to the pre- and post-monsoon periods.

In contrast, BC is a primary emission product of combustion that may originate from both local and distant sources. The early morning peak during all three seasons suggests possible contributions from the local combustion of biofuels for cooking and heating, which are most prevalent during early morning. The secondary peak in the afternoon and early evening occur when the local anthropogenic sources are at miminum in the KGV. Up-valley air transports air mass from the plains via valley wind system analogous to "Alpine pumping". As discussed in more detail below, the local wind fields within the KGV appear to have driven diurnal variability in BC.

3.3 Evolution of local wind system in the KGV

Theodolite observations at different locations along the KGV in 1998 show minor shifts - less than 45° - in wind direction and less than 2 m s^{-1} in wind speed in the lower 1000 m above the surface during daytime (Egger et.al 2000). However at nighttime, deviation in wind speed and direction from daytime conditions is expected due to strong nocturnal stratification. At approximately 900 m above the valley floor, JSM2 is likely to be within the residual layer during nighttime. Measurements at the four AWS stations on the valley floor illustrate the evolution of surface wind velocities at variuos locations within the KGV (Fig. 4). Comparison between the short term record for 8 to 14 May 2015 at JSM2 (Fig. 4) and the longer-term record for the entire month May 2013 at JSM1 (Supplement) reveal that velocities at the higher elevation site were about 5 m s^{-1} greater than those near the valley floor but with similar

Atmos. Chem. Phys. Discuss., doi:10.5194/acp-2016-824, 2016
Manuscript under review for journal Atmos. Chem. Phys.
Published: 8 November 2016

Atmospheric Chemistry and Physics Discussions

diurnal cycles. Although wind velocites at JSM2 varied somewhat over the year, all months exhibited similar diurnal patterns that evolved seasonally as a function of sunrise and sunset (Supplement).

Air flow along the valley is driven by gradients in temperature and pressure between the entrance and the exit regions of the valley. The windroses (Fig. 4a) illustrate the temporal evolution of up- and down-valley flows along the valley floor. At Jomsom, up valley flows are southwesterly and dominant during daytime with peak velocities of 10 to 15 m s^{-1} between about 0900 LT to 1800 LT. The wind velocites along the valley peaked within the core of the valley at MPH and JSM2 and were lower at the entrance (LET) and exit (EKL) regions (Fig. 4b). The duration of strong wind speeds within the valley during daytime supports the hypothesis that wind flow is modulated by the pressure gradient created as a result of differential heating of the arid valley floor relative to the mouth of the valley. The finding is in agreement with that of Egger et al. (2000) that the wind velocity is driven by the gradient in temperature thus pressure between the entrance and the exit regions of the valley. Wind velocities decreased substantially after 1800 LT, with variable wind direction possibly due to the influence of down-slope flows in the valley when the down-valley flows were weak.

3.4 Local wind drivers of BC and O_3 in the KGV

Figure 6 shows the time series of BC and O_3 during individual months (April/pre-monsoon, July/monsoon, November/post-monsoon) that are representative of each season. For both pre-monsoon and monsoon periods, BC concentrations peaked at 0700 LST (Fig. 4) when wind velocities were low (Fig. 5). This peak occurred about an hour later during the post monsoon period, with all seasons experiencing decrease in BC over the rest of the morning as wind speeds increase (Fig. 4). Calm wind speed, higher use of biofuel burning for cooking and slowly decaying nocturnal boundary layer in the morning limit emission flow close to the source. Assuming that the early morning peak reflects contributions from local sources, decreasing concentrations with increasing wind speeds are consistent with expectations based on dilution. Thereafter, concentrations increased over the afternoon and early night, reaching secondary peaks near midnight LST during the pre-monsoon and several hours earlier during other periods (Fig. 4 and 6). The secondary peaks are the result of mountain-valley wind system pumping air from over the plains through the KGV. Ozone exhibits a distinct minimum in the early morning. However, mixing ratios increase during the morning, peak in the early afternoon well before that of BC and decrease over night.

Interseasonal variability in the timing of the morning BC peak is likely related to seasonal changes in sunrise and corresponding temporal changes to thermal-driven pressure gradients coupled with shifts in daily activities and associated emissions such as cooking and heating with biofuels. BC measurements at the JSM-STA - on the east-facing slope of the valley - suggest that strong upslope flows in the morning coincide with weaker down-valley flow and higher local pollution from cooking. These strong upslope morning flows likely transport the local pollution upslope rather than up-valley, while during

Atmos. Chem. Phys. Discuss., doi:10.5194/acp-2016-824, 2016
Manuscript under review for journal Atmos. Chem. Phys.
Published: 8 November 2016

Atmospheric Chemistry and Physics Discussions

the day after the boundary layer is fully developed strong up-valley flows occur (Fig. 5). Dilution of local emissions associated from increasing wind speed likely contributes to decreasing BC concentration during late morning.

In addition to the wind pattern, the growth of the boundary layer also affects surface concentration. Noctural decoupling of the boundary layer preserves the concentration of both O_3 and BC in the valley from the previous day. A shallow morning boundary layer in conjunction with stronger upslope flows and emissions from biofuel burning increases surface concentrations of BC, while the strong wind speed along with the growing boundary layer strengthens the dilution effect in the valley. These diurnal patterns are occasionally replaced by periods of high BC or O_3 in the pre- and post-monsoon seasons.

3.4 Evidence of transport episodes in valley concentration

3.4.1 BC and O_3 concentration anomaly

Along with the regular diurnal and seasonal variability described above, we also observed anomalous periods when for several days concentrations of both BC and O_3 were significantly greater than their corresponding monthly averages. These extended periods of high BC and O_3 are possible evidence of large scale transport from the IGP to the TP via trans-Himalayan valleys. This assertion is reasonable because we assume that most pollution from local sources only occurs in the morning and is diluted by increased wind speed by mid-day. We identified three common patterns/transport episodes seen in the KGV (Figure 6).

During the regional transport episode in May 2013 (pattern A), average BC concentration (2.45 µg m^{-3}) was 102% higher than the 2-year average concentration, 1.21 µg m^{-3}, for the month (Fig. 6). The corresponding O_3 concentration (58.37 ppbv) was 10% higher that the 2-year monthly average (53.26 ppbv). The MODIS fire data showed more than 100 fire events in the Punjab region of India for 5 out of 10 days during that period (Fig. 7a). The fire sources in Punjab during May 2013 is about 800 km away from Jomsom. The pollutants emitted from this crop residue burning increased BC concentration in the KGV valley from 0.8 µg m^{-3} to 2.08 µg m^{-3} as shown in figure 6. BC in the valley increased steadily from May 2nd until it reached over 4 µg m^{-3} on the 5th of May. This elevated concentration of BC persisted for 10 days.

The mean BC concentration during the regional transport episode in June (pattern B) was 125% higher than the average monthly mean for June (1.01 µg m^{-3}) while the mean O_3 mixing ratio (69.97 ppbv) exceeded the monthly mean (47.23 ppbv) by 45%. Again, during this time, MODIS fire imagery identified fires events in the foothills of the Himalaya in Western Nepal, about 300 km from KGV (Fig. 7b). However, though both patterns A and B appear to have resulted from extensive burning in the

Atmos. Chem. Phys. Discuss., doi:10.5194/acp-2016-824, 2016
Manuscript under review for journal Atmos. Chem. Phys.
Published: 8 November 2016

Atmospheric Chemistry and Physics Discussions

region, pattern B showed a slower rise in BC concentration in the valley and lasted for 5 days. The proximity to fire sources differentiated pattern A from pattern B.

Pattern C shows higher O_3 and BC concentrations as a result of extensive haze over IGP during Dec. 2014 (Fig. 6). The mean BC concentration during pattern C (1.14 µg m^{-3}) was 45% higher than the monthly average (0.78 µg m^{-3}) whereas O_3 mixing ratio decreased 10% from 33.19 ppbv monthly average to 30.02 ppbv. This suggests that the extensive haze during this period (Fig. 7c) attenuated incident solar radiation, thereby slowing the net photochemical production of O_3.

The regional transport episodes highlighted above frequently occurred in the pre- and post-monsoon seasons when the synoptic winds are southwesterly, from the IGP, and wet deposition from precipitation is negligible. The local wind system of the Himalayan valleys is well-developed, and is the most important driving factor for the flow of air into the valleys. Emissions from crop residue burning and natural fires occur in the pre- and post-monsoon season, in addition to the regular, year-round emission sources like industries and vehicles. During agricultural crop residue burning, BC concentration peaks reached over 20 µgm^{-3} in Northern India (Khoral et al, 2012) which was similar to corresponding daily BC concentration peak observed in Kathmandu, Nepal (Putero et al, 2015). Agricultural burning significantly contributes to high BC in the region during April-May and October-November, while forest fires are common in March-April. The MODIS fire product shows March through June as major fire season with about 2500 fire counts in the lower Himalaya, annually (Vadrevu et al., 2012). Lower temperatures in the winter season are responsible for more shallow boundary layers that confine the pollutants near the surface where they accumulate as a result of limited convection which results in the formation of haze in the region. All the above factors contribute to the elevated BC and O_3 concentration in the air, transported via the Himalayan valleys to higher elevations. Observations show that about 266 µg m^{-2} of BC is deposited in the higher Himalaya during the pre-monsoon season, March-May (Yasunari et al., 2010).

3.4.2 Pollution in the Higher Himalaya

BC concentrations in European cities like Barcelona, Lugano and London range between 1.7 to 1.9 µg m^{-3} (Reche et al., 2011). National Ambient Air Quality Standards (NAAQS) for the United States for O_3 is 70 ppbv (8-hour maximum average). During regional transport episodes, BC and O_3 levels in the remote site in Jomsom exceeded the above levels for both BC and O_3 ocassionally. BC and O_3 concentrations suggest that the extensive haze layer over the IGP during pre-monsoon along with increased fire activity in the IGP and Himalayan foothills results in an increased flux of pollutants into the Himalayan valleys (Fig 6 and 7). The pollutants are transported by the local wind system, specifically the up valley winds that are dominant throughout the day. Further analysis is needed to understand probable oscillation or stagnation of polluted air mass trapped in the valley as no dominant down valley flow was seen at nighttime in the valley floor except for at the entrance region, Lete. There

Atmos. Chem. Phys. Discuss., doi:10.5194/acp-2016-824, 2016
Manuscript under review for journal Atmos. Chem. Phys.
Published: 8 November 2016

Atmospheric Chemistry and Physics Discussions

is a strong possibility that the transported pollutants are stagnant at nighttime and are transported further up the valley when the nocturnal boundary layer dissolves and the strong up valley flow resumes. Stratospheric intrusions also influence the relative abundance of O_3 and BC in the high-elevation Himalaya. Deep monsoon convection causes enhanced mass flux across the tropopause when the vertical temperature gradient is weak. This mass flux across the tropopause causes strong downdraft around the tropopause causing stratospheric exchange in mid-latitudes (Kumar, 2006). Conditions for STE over the Himalaya is possible when the monsoon air masses move towards the Himalaya. Signatures of stratospheric intrusions have been observed at NCO-P during all seasons but predominantly during pre-monsoon and post monsoon season (Bracci et al., 2011).

4. Conclusion

This study provides the first in-situ observational evidence of the role of trans-Himalayan valleys as prominent pathways for air pollution transport from the IGP to the TP. The concentrations of BC and O_3 in the KGV exhibited systematic diurnal and seasonal variability. During the non-monsoon months, we observed episodes of high pollutant transport through the KGV. Our results suggest that transport through trans-Himalayan valleys during episodic periods of regional pollution over the IGP accounts for disproportionately large fractions of total BC transport from southern Asia to the Tibetan Plateau.

Further studies should be conducted to understand the vertical and horizontal distribution of particulate matter and ozone in the Himalayan region. Further investigation particularly using sondes and LiDar could help understand the stratification of the vertical air masses. Our findings here can enhance the predictive capabilities of the scientific communities in analyzing the impacts of increasing air pollution in the Himalayan region, on human health, food security, economies, and available natural resources along with estimating the flux of pollutants through the Himalayan valleys.

Acknowledgments

We would like to acknowledge our field assistant in Nepal, Buddhi Lamichhane who helped us in various stages of the study, as well as the logistic and administrative support and internet at the Jomsom station provided by Nepal Wireless. Financial support was provided by the National Aeronautics and Space Administration NNX12AC60G, and additional field support was provided by ICIMOD's Atmosphere Initiative. The authors are very thankful for comments from William Keene and Jennie Moody.

Atmos. Chem. Phys. Discuss., doi:10.5194/acp-2016-824, 2016
Manuscript under review for journal Atmos. Chem. Phys.
Published: 8 November 2016

References

Auffhammer, M., Ramanathan, V. and Vincent, J. R.: Integrated model shows that atmospheric brown clouds and greenhouse gases have reduced rice harvests in India, *PNAS* 10.1073/pnas.0609584104, 2006.

Bracci, A., Cristofanelli, P., Sprenger, M., Bonafe, U., Calzolari, F., Duchi, R., Laj, P., Marinoni, A., Roccato, F., Vuillermoz, E., Bonasoni, P.: Transport of Stratospheric Air Masses to the Nepal Climate Observatory–Pyramid (Himalaya; 5079 m MSL): A Synoptic-Scale Investigation, *J Appl. Meteorol. Clim.*, 51,1489-1507, 2013.

Brun, J., Shrestha, P., Barros, A., P.: Mapping aerosol intrusion in Himalayan valleys using the Moderate Resolution Imaging Spectroradiometer (MODIS) and Cloud Aerosol Lidar and Infrared Pathfinder Satellite Observation (CALIPSO), *Atmos. Env.*, 45 (2011) 6382-6392, 2011.

Bonasoni, P., Cristofanelli, P., Marinoni, A.,Vuillermoz, E.: Atmospheric Pollution in the Hindu Kush – Himalaya Region. *Mountain Research and Development*, *32*(4), 468–479. http://doi.org/10.1659/MRD-JOURNAL-D-12-00066.1, 2012.

DOTM-Vehicle data zonal wise till 2072 baishakh, Government of Nepal, Department of Transportation Management (http://www.dotm.gov.np/uploads/files/Vehicle-data-zonal-wise-till-2072-baishakh.pdf) accessed March 26th, 2016.

Egger, J., Bajracharya, S., Egger, U., Heinrich, R., Reuder, J., Shakya, P., Wendt, H., and Wirth, V.: Diurnal winds in the Himalayan Kali Gandaki valley. Part I: observations, *Mon. Weather Rev.*, 128, 1106-1122, 2000.

Egger, J., Bajracharya, S., Egger, U., Heinrich, R., Kolb, P., Lammlein, S., Mech, M., Reuder, J., Schaper, W., Shakya, P., Schween, J. and Wendt, H.: Diurnal winds in the Himalayan Kali Gandaki valley. Part III:remotely piloted aircraft soundings, *Mon. Weather Rev.*, **130,** 2042-2058, 2002.

Engling, G., and Galencser, A.: Atmospheric brown clouds: from local air pollution to climate change, *Elements*, 6, 223-228, 2010.

Gustafsson, O., Kruså, M., Zencak, Z., Sheesley, R., J., Granat, L., Engström,E., Praveen, P., S., Rao, P., S., P., Leck, C., Rodhe, H.: Brown Clouds over South Asia: Biomass or Fossil Fuel Combustion?, *Science*, 323, 495-498, 2009.

Jacobson, M., Z.: Strong radiative heating due to the mixing state of black carbon in atmospheric aerosols, *Nature*, 409, 695-697, 2001.

Janssen, Nicole A. H., Hoek, G., Simic-Lawson, M., Fischer, P., van Bree, L., Brink, H., Keuken, M., Atkinson, R. W., Anderson, H. R., Brunekreef, B., and Cassee, F. R.: Black carbon as an additional

indicator of the adverse health effects of airborne particles compared with PM_{10} and $PM_{2.5}$, *Environ. health persp.* 119 (12), 1691-1698, 2011.

Kang, S., Xu, Y., You, Q., Flugel, W-A., Pepin, N. and Yao, T. review of Climate and cryospheric change in the Tibetan Plateau, *Environ. Res. Lett.* 5(1), 015101, 2010.

Kaufman, Y. J., Tanré, D., and Boucher, O.: A satellite view of aerosols in the climate system, *Nature*, 419, 215–223, 2002.

Kharola, S., K.,Badarinath, K., V., S.,, Sharma, A., R., Mahalakshmi, D. V., Singh, D., Prasad, V. K.: Black carbon aerosol variations over Patiala city, Punjab, India—A study during agriculture crop residue burning period using ground measurements and satellite data, *J. Atmos. Sol.-Terr. Phys.*, 84-85, 45-51, 2012.

Kopacz, M., Mauzerall,D., L., Wang, J.,Leibensperger, E., M., Henze, D., K., and K. Singh, K.: Origin and radiative forcing of black carbon transported to the Himalayas and Tibetan Plateau, *Atmos. Chem. Phys.*, 11, 2837–2852, 2011.

Krupnick, A., J., Harrington, W., Ostro, B.: Ambient ozone and acute health effects: Evidence from daily data, *J. Environ. Econ. Manag.*, 18(1), 1-18, 1990.

Kumar, K. K., 2006: VHF radar observations of convectively generated gravity waves: Some new insights, Geophys. Res. Lett., 33, L01815, doi:10.1029/2005GL024109.

Lau, K., M., Kim, M., K., Kim, K., M.: Asian summer monsoon anomalies induced by aerosol direct forcing: The role of the Tibetan Plateau, *Climate Dynamics*, 26, 855–864, 2006.

Lawrence, M. G. and Lelieveld, J.: Atmospheric pollutant outflow from southern Asia: a review, *Atmos. Chem. Phys.*, 10, 11017–11096, doi:10.5194/acp-10-11017-2010, 2010.

Lee K, Soon DH, Shugui H, Sungmin, Xiang Q, Jaiwen R, Yapping L, Rosmann KJRR, Barbante C, Bourton CF.: Atmospheric pollution of trace elements in the remote high-altitude atmosphere in Central Asia as recorded in snow from Mt Qomolangma (Everest) of the Himalayas, *Sci. Tot. Environ.* 404, 171-181, 2008.

Lu, Z., Zhang, Q., and Streets, D., G.: Sulfur dioxide and primary carbonaceous aerosol emissions in China and India, 1996–2010, *Atmos. Chem. Phys.*, 11, 9839-9864, 2011.

Luthi, Z., L., Skerlak, B., Kim, S., W., Lauer, A., Mues, A., Rupakheti, M., and Kang, S.: Atmospheric brown clouds reach the Tibetan Plateau by crossing the Himalayas, *Atmos. Chem. Phys.*, 15, 11, 6007-6021, 2015.

Ma, J., Chen, Y., Wang, W., Yan, P., Liu, H.,Yang, S., Hu, Z., and Lelieveld, J.: Strong air pollution causes widespread haze-clouds over China, *J. Geophys. Res.*, 115, D18204, 2010.

Marinoni, A., Cristofanelli, P., Laj, P., Duchi., Putero, D., Calzolari, F., Landi., T., C., Vuillermoz, E., Maione, M., Bonasoni, P.: High black carbon and ozone concentrations during pollution transport in the Himalayas: Five years of continuous observations at NCO-P global GAW station, *J. Environ. Sci.*, 25(8) 1618–1625, 2013.

Menon, S., Hansen, J., Nazarenko, L. and Yunfeng, L.: Climate Effects of Black Carbon Aerosols in Aerosols in China and India, *Science*, 297, 2250-2253, 2002.

Piketh, S. J., Annegarn, H., J., and Tyson, P., D.: Lower tropospheric aerosol loadings over South Africa: The relative contribution of aeolian dust, industrial emissions, and biomass burning, *J. Geophys. Res.*, 104(D1), 1597–1607, 1999.

Putero, D., Cristofanelli, P., Marinoni, A., Adhikary, B., Duchi, R., Shrestha, S. D., Verza, G. P., Landi, T. C., Calzolari, F., Busetto, M., Agrillo, G., Biancofiore, F., Carlo, P. Di., Panday, A. K. , Rupakheti, M., and Bonasoni, P.: Seasonal variation of ozone and black carbon observed at Paknajol, an urban site in the Kathmandu Valley, Nepal, *Atmos. Chem. Phys*., 15, 13957–13971, 2015.

Ramanathan, V., and Carmichael, G.: Global and regional climate changes due to black carbon, *Nat. Geosci.*, 1(4), 221–227, 2008.

Ramanathan, V., Chung, C., Kim, D., Bettge, T., Buja, L., Kiehl, J., T., Washington, W., M., Fu, Q., Sikka, D., R., and Wild, M.: Atmospheric brown clouds: Impacts on South Asian climate and hydrological cycle, *PNAS*, 102(15), 5326-5333, 2005.

Ramachandran, S., Rajesh, T., A.: Black carbon aerosol mass concentrations over Ahmedabad, an urban location in western India: Comparison with urban sites in Asia, Europe, Canada, and the United States, *J Geophys. Res-Atmos.*112(D06211), doi/10.1029/2006JD007488, 2007.

Ramanathan, V., Ramana, V., M., Roberts, G., Kim, D., Corrigan, C., Chung, C., Winker, D.: Warming trends in Asia amplified by brown cloud solar absorption, *Nature*, 448(2), 575-578, 2007a.

Ramanathan, V., Li, F., Ramana, M.V., Praveen, P.S., Kim, D., Corrigan, C.E., Nguyen, H., Stone, E.A., Schauer, J.J., Carmichael, G.R., Adhikary, B., Yoon, S.C.: Atmospheric Brown Clouds: Hemispherical and Regional Variations in Long-Range Transport, Absorption, and Radiative Forcing, *J. Geophys. Res.*, 112, D22821, 2007b.

Reche, C., Querol, X., Alastuey, A., Viana, M., Pey, J., Moreno, T., Rodríguez, S., González, Y., Fernández-Camacho, R., De La Campa, A. M, Sálnchez,De La Rosa, J., Dall'Osto, M., Prévôt, A. S H, Hueglin, C., Harrison, R. M., Quincey, P.: New considerations for PM, Black Carbon and particle number concentration for air quality monitoring across different European cities, *Atmos. Chem.*

Phys., 11, 6207–6227, 2011.

Reiter, E. R., and Tang, M.: Plateau effects on diurnal circulation patterns. *Mon. Wea. Rev.*, 112, 638–651, 1984.

Sreekanth, V., Niranjan, K., Madhavan, B. L.: Radiative forcing of Black Carbon over Eastern India, *Geophys. Res. Lett.*, 34(L17818), doi: 10.1029/2007GL030377, 2007.

Steinacker, R.: Area–height distribution of a valley and its relation to the valley wind, Beitr. Phys. Atmos., 57, 64–71, 1984.

Whiteman, C. D., and Bian X.: Use of radar profiler data to investigate large-scale thermally driven flows into the Rocky Mountains, *Proc. Fourth Int. Symp. on Tropospheric Profiling: Needs and Technologies*, Snowmass, CO, 1998.

Weissmann, M., Braun, A. F. J., Gantner, A., L., Mayr, A., G., J.,Rahm, A., S., Reitebuch, A., O. :The Alpine Mountain–Plain Circulation: Airborne Doppler Lidar Measurements and Numerical Simulations, *Mon. Weather Rev.*, 133,(11), 3095-3109, 2005.

Vadrevu, K., P., E., K., V., S., Vermote, E.: MODIS derived fire characteristics and aerosol optical depth variations during the agricultural residue burning season, north India, *Environ. Pollut.*, 159(6), 1560–1569, 2011.

Vasilyev, O. B., Contreras, A., L., Velazquez, A., M., Fabi, R., P., Ivlev, L., S., Kovalenko, A., P., Vasilyev, A., V., Jukov, V., M., and Welch, R., M.: Spectral optical properties of the polluted atmosphere of Mexico City (spring-summer 1992), *J. Geophys. Res.*, 100(D12), 26027–26044, 1995.

Yasunari, T. J., Bonasoni, P., Laj, P., Fujita, K., Vuillermoz, E., Marinoni, A., Cristofanelli, P., Duchi, R., Tartari, G., and Lau, K., M.: Estimated impact of black carbon deposition during pre-monsoon season from Nepal Climate Observatory - Pyramid data and snow albedo changes over Himalayan glaciers, *Atmos. Chem. Phys.*, 10(6), 603-6,615, 2010.

Wang, X. and Mauzerall, D. L.: Characterizing distributions of surface ozone and its impact on grain production in China, Japan and South Korea: 1990 and 2020, *Atmos. Environ.* 38, 4383-4402, 2004.

Xu, C., Ma, Y. M., You, C., and Zhu, Z. K.: The regional distribution characteristics of aerosol optical depth over the Tibetan Plateau, *Atmos. Chem. Phys*., 15, 12065–12078, 2015.

Zangl, G., Egger, J., and Wirth, V.: Diurnal Winds in the Himalayan Kali Gandaki Valley. Part II: Modeling, *Mon. Weather Rev*., 129, 1062-1080, 2000.

Atmos. Chem. Phys. Discuss., doi:10.5194/acp-2016-824, 2016
Manuscript under review for journal Atmos. Chem. Phys.
Published: 8 November 2016

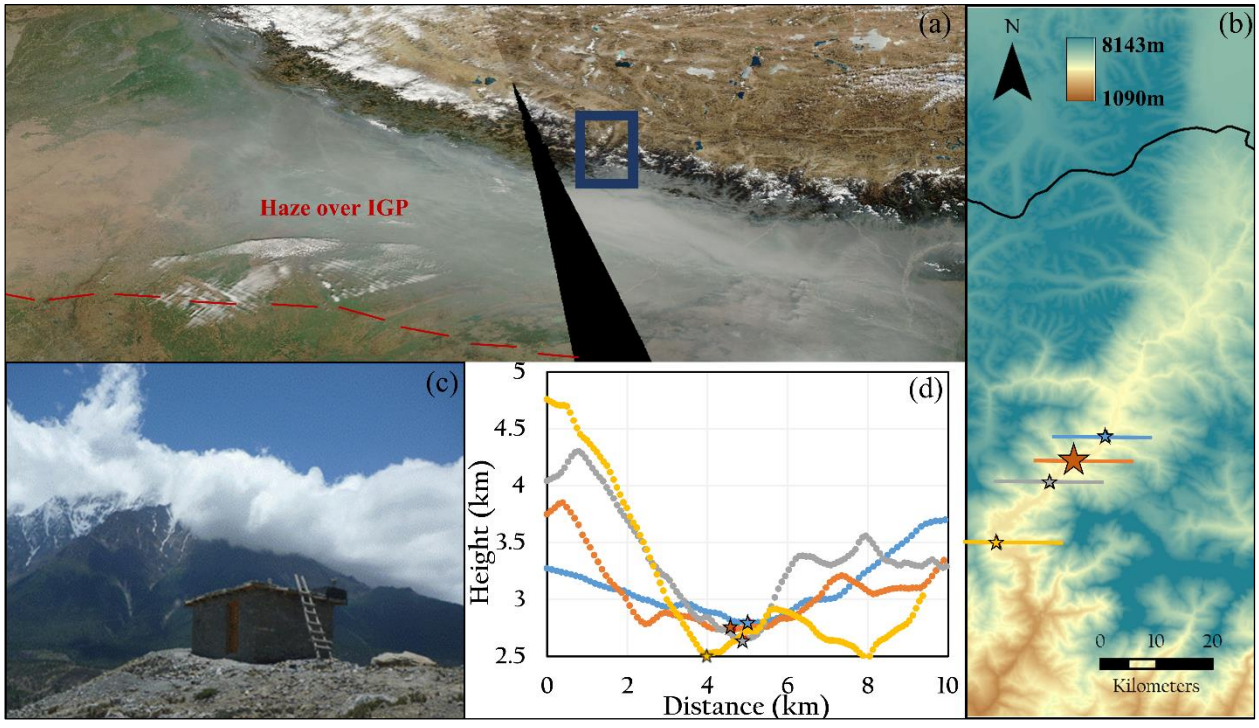

Figure 1. (a) NASA Worldview image from January 15th, 2013 depicting thick haze over IGP. The KGV lies within the boxed (blue) region, the red dashed line shows the extent of the haze and the black triangle is the data gap in the imagery. (b) Expanded scale of the KGV showing locations of LET near the entrance of the valley (yellow star); MPH in the core region (gray star); the JSM_STA sampling station for BC and O_3 and the two associated AWS sites (JSM_1 and JSM_2) in the core region (orange star); and EKL near the exit (blue star). (c) The atmospheric observatory at Jomsom (JSM_STA). (d) Cross-sectional elevation profile at the indicated locations.

535

Atmos. Chem. Phys. Discuss., doi:10.5194/acp-2016-824, 2016
Manuscript under review for journal Atmos. Chem. Phys.
Published: 8 November 2016

Atmospheric Chemistry and Physics Discussions

Station	Location	Elevation	Instrument
JSM_STA	28.87N, 83.73E	2850m	Thermo BC MAAP (Model 5012)
JSM_STA	28.87N, 83.73E	2850m	2B Tech Ozone instrument (Model 205)
JSM_1	28.87N, 83.73E	2800m	DAVIS (Model Vantage Pro 2)
JSM_2	28.87N, 83.73E	3700m	NexSens (Model Vaisala WXT520)
LET	28.93N, 83.35E	2500m	Nexsens (ModelVaisala WXT520)
MPH	28.44N, 83.41E	2665m	HOBO (Model AWS U-30)
EKL	28.49N, 83.46E	2804m	NexSens (ModelVaisala WXT520)

Table 1. Location of the atmospheric station and weather stations along the KGV.

Atmos. Chem. Phys. Discuss., doi:10.5194/acp-2016-824, 2016
Manuscript under review for journal Atmos. Chem. Phys.
Published: 8 November 2016

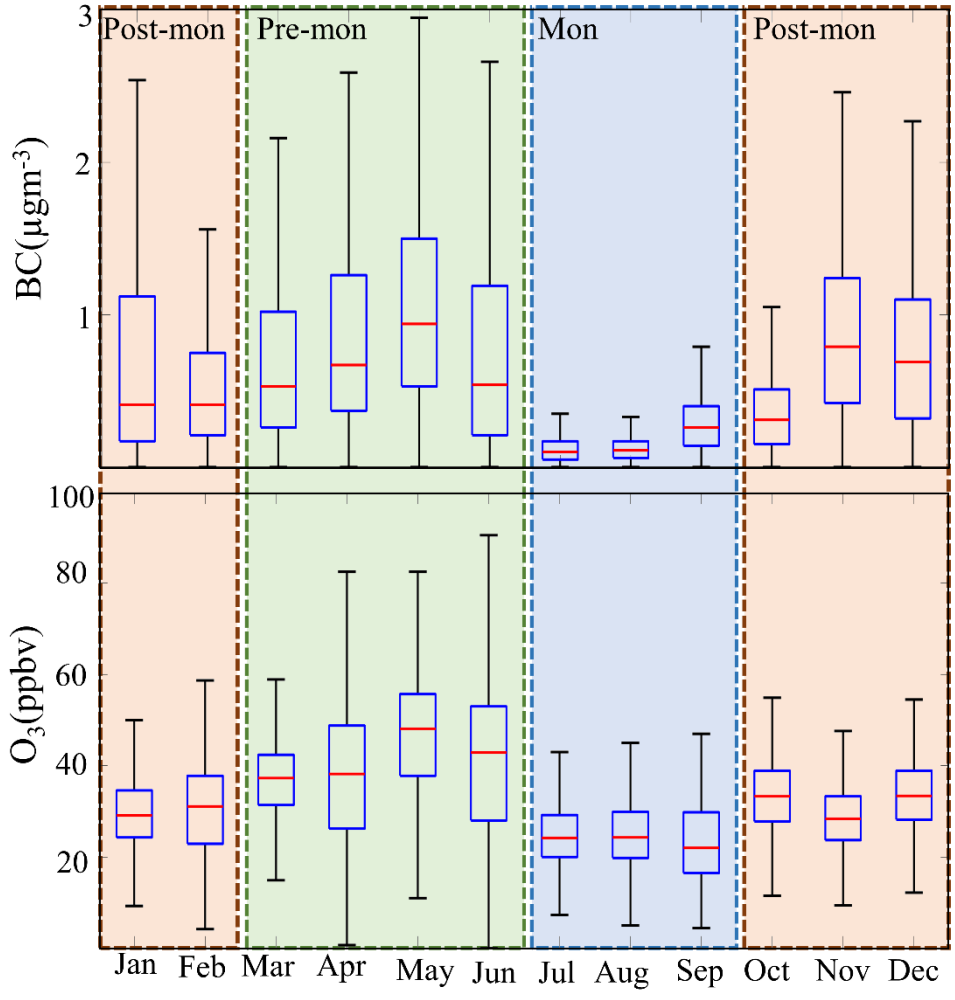

Figure 2. Box and whisker plots depicting the 90th, 75th, 50th, 25th, and 10th percentiles for monthly concentrations of BC (upper panel) and O_3 (lower panel) between January 2013 and August 2015 at JSM_STA. Orange shaded areas indicate the post-monsoon season (Post-mon), green shaded area indicates the pre-monsoon (Pre-mon) and blue are indicates the monsoon (Mon) season.

Atmos. Chem. Phys. Discuss., doi:10.5194/acp-2016-824, 2016
Manuscript under review for journal Atmos. Chem. Phys.
Published: 8 November 2016

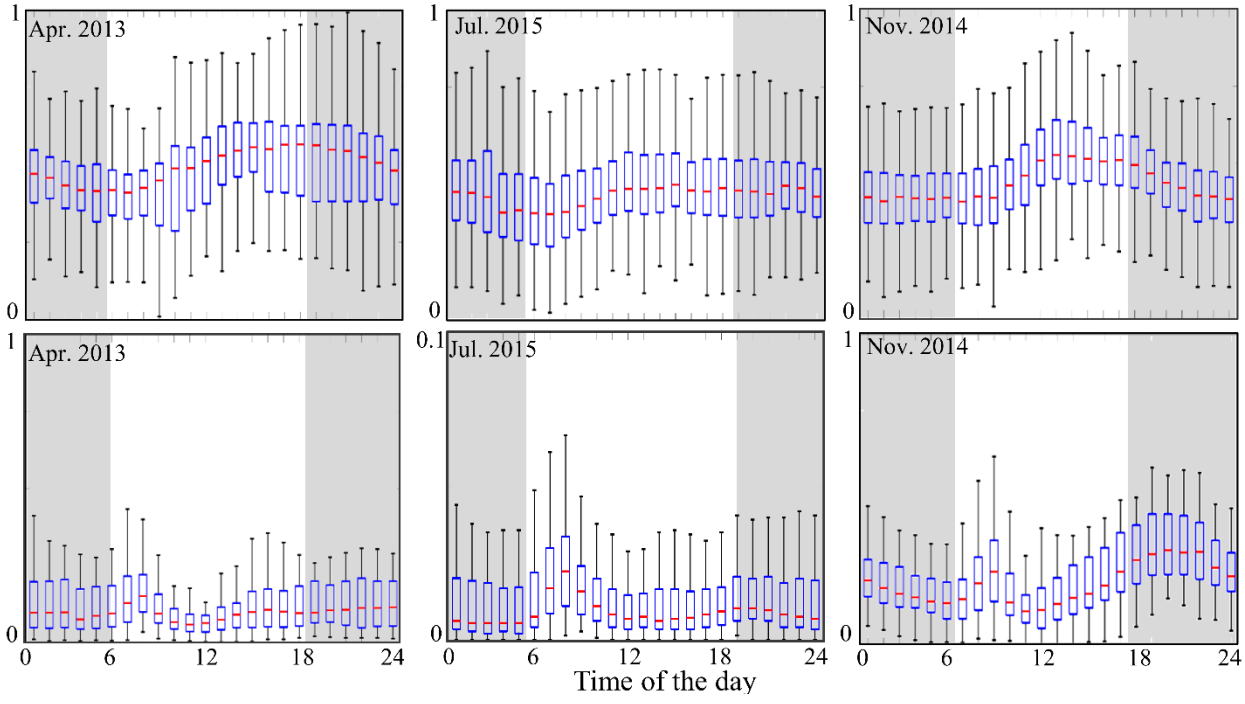

Figure 3. Box and whisker plots depicting the 90th, 75th, 50th, 25th, and 10th percentiles for normalized diel variability in O_3 (upper panels) and BC (lower panels) at JSM_STA during April 2013 (pre-monsoon), July 2015 (monsoon), and November 2014 (post-monsoon). Scale for July 2015 is from 0 to 0.1.

Atmos. Chem. Phys. Discuss., doi:10.5194/acp-2016-824, 2016
Manuscript under review for journal Atmos. Chem. Phys.
Published: 8 November 2016

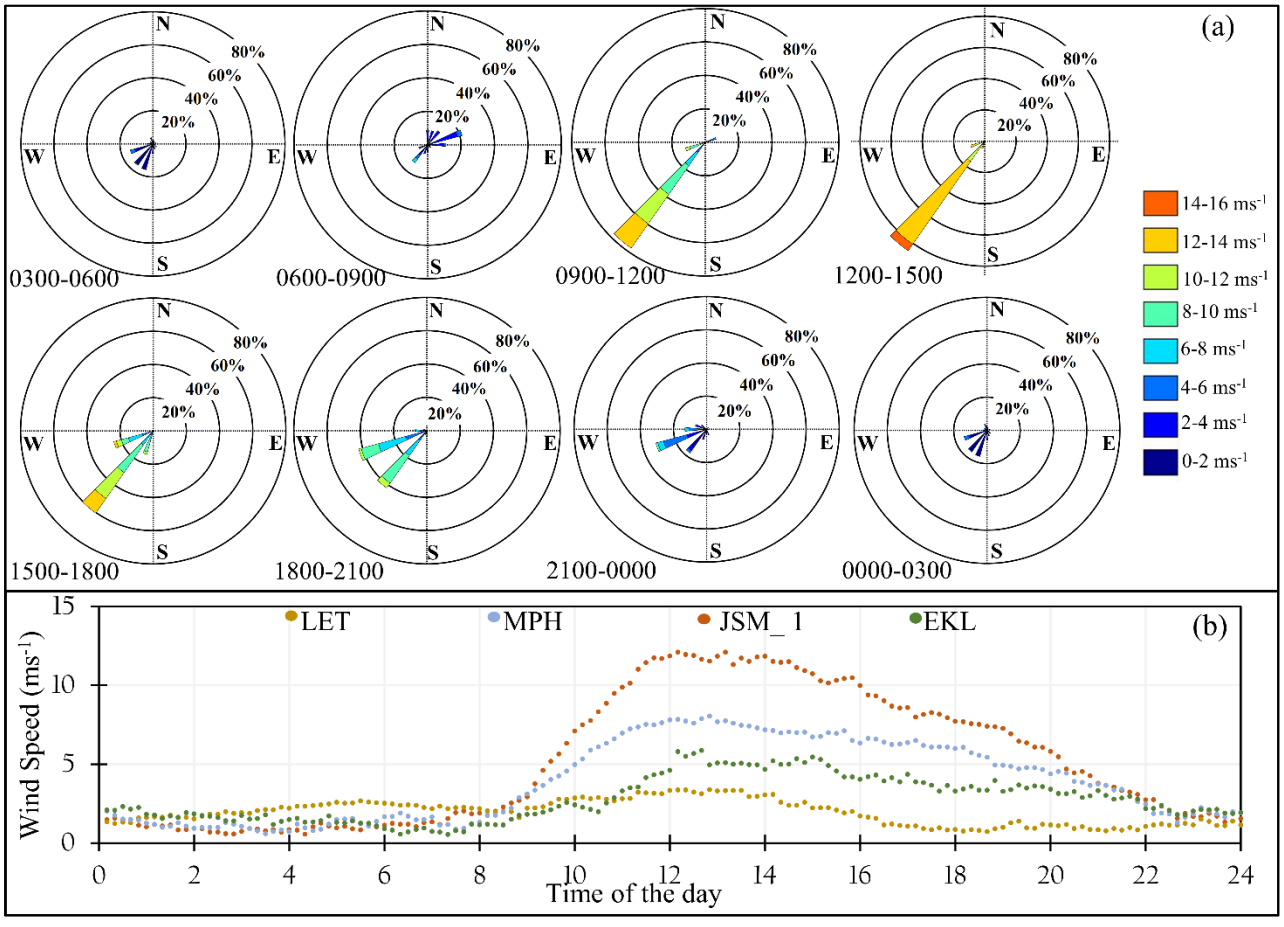

Figure 4. (a) Wind rose for data from May 8 to 14, 2015 binned into 3-hour increments depiciting diurnal evolution in wind speed and direction at JSM_2. (b) Corresponding diurnal variability in wind speed based on average values over the same period at LET, MPH, JSM_2 and EKL.

620

Atmos. Chem. Phys. Discuss., doi:10.5194/acp-2016-824, 2016
Manuscript under review for journal Atmos. Chem. Phys.
Published: 8 November 2016

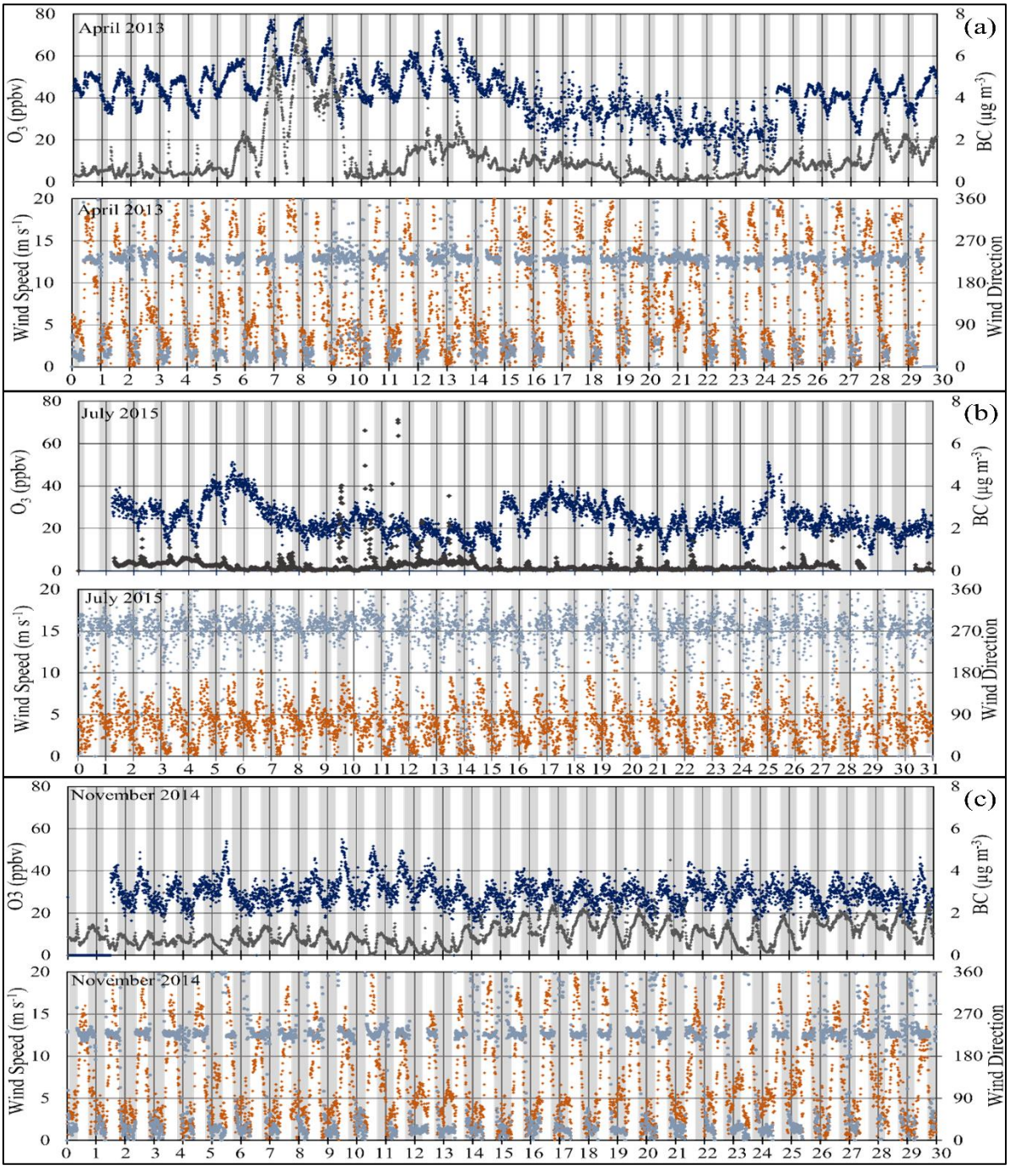

Figure 5. Variation in O_3, BC, and associated wind speed and direction at JSM_STA during (a) April 2013 (pre-monsoon), (b) July 2015 (monsoon), and (c) November 2014 (post monsoon). The grey shaded area denotes night.

Atmos. Chem. Phys. Discuss., doi:10.5194/acp-2016-824, 2016
Manuscript under review for journal Atmos. Chem. Phys.
Published: 8 November 2016

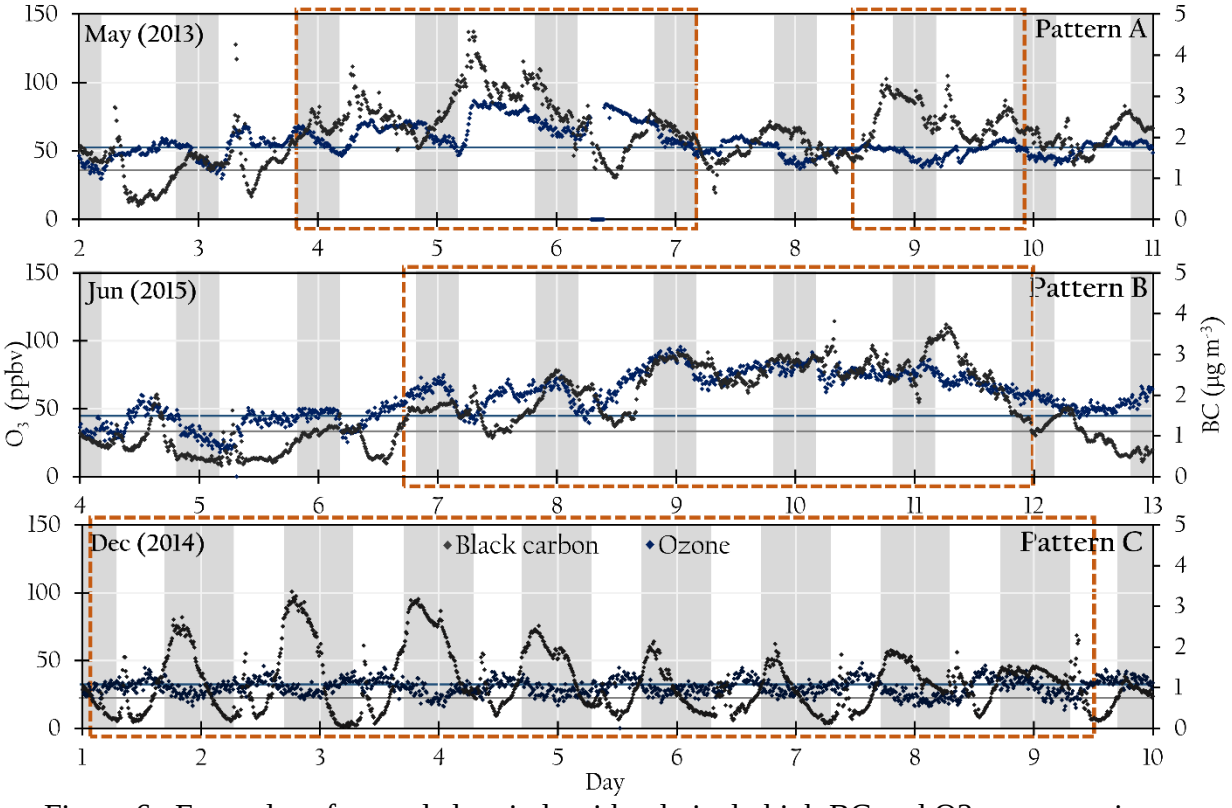

Figure 6. Examples of extended periods with relatively high BC and O3 concentrations at JSM_STA during the pre-monsoon months of May 2015 (Pattern A) and June 2015 (Pattern B and the post-monsoon month of December 2014 (Pattern C). The solid blue and grey lines depict two-year averages for O3 and BC, respectively, and the orange boxes bracket the indicated pattens.

655

Atmos. Chem. Phys. Discuss., doi:10.5194/acp-2016-824, 2016
Manuscript under review for journal Atmos. Chem. Phys.
Published: 8 November 2016

Atmospheric Chemistry and Physics Discussions

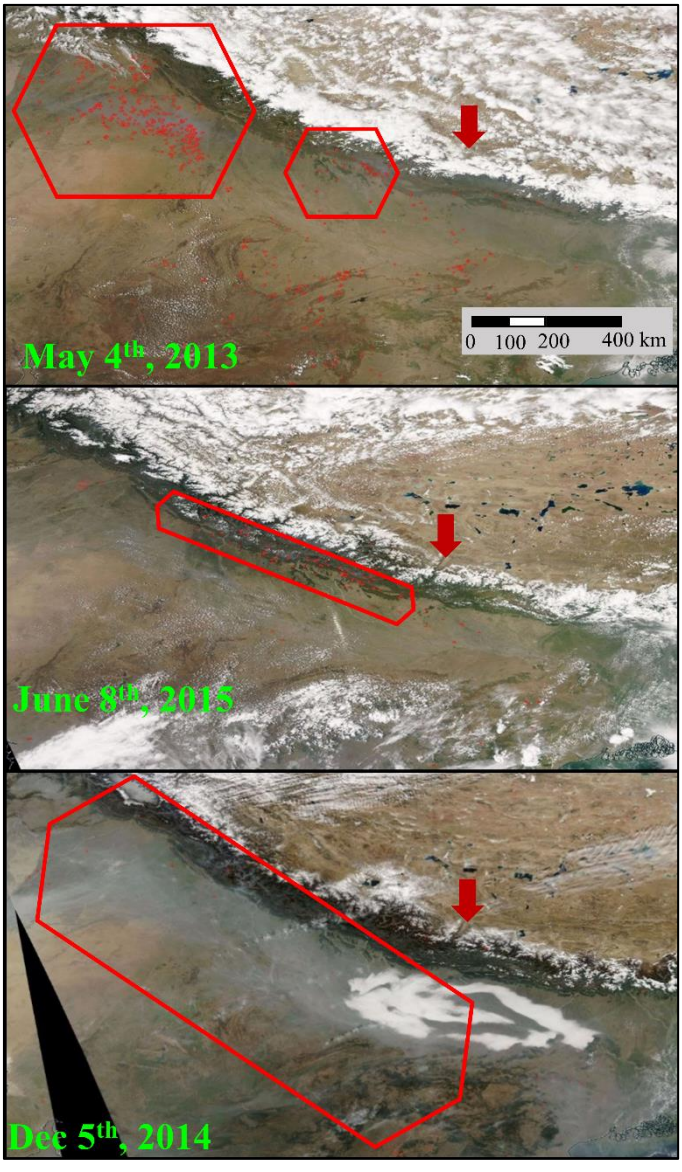

Figure 7 MODIS imagery depicting haze and individual fire events during the regional transport episodes associated with the patterns depicted in Figure 7. The red arrows point to the KGV.